ARTICLE

Received 00th January 20xx,
Accepted 00th January 20xx

DOI: 10.1039/x0xx00000x

Orientation preference control: a novel approach for tailoring molecular electronic functionalities

Xintai Wang,[a,b,c,†] Xiaoying Li,[a*] Shanglong Ning,[b,†] and Ali Ismael[d*,e,†]

ABSTRACT: Molecular wires with asymmetric anchors have garnered considerable interest in the field of molecular electronics. Numerous studies have focused on asymmetrically anchored molecules, both at the single molecule and self-assembled monolayer (SAM) scales. However, few studies have investigated how the binding preference of asymmetric anchors towards the substrate affects their quantum transport behaviour. In this study, Oligo (arylene ethynylene) derivatives with thiol acetate anchors at one terminal and pyridine anchors at the other terminal were used for self-assembly, gold and single-layered graphene (SLG) were employed as the bottom and top electrodes to form molecular junctions. XPS results indicated that, without deprotecting acetyl group on thiol acetate, the molecules tended to assemble on Au either with thiol anchor or pyridine anchor. However, with the deprotection procedure (which transformed the thiol acetate into thiol), almost all molecules tended to assemble on Au with thiol anchor. Further quantum transport measurements revealed that both the electron tunnelling efficiency and the energy difference between the electrode Fermi level and the molecular frontier orbital had also shifted due to this change in binding preference. For example, the field effect transistor behaviour of functional SAMs can be switched between ambipolar (where the molecule can be turned on by shifting the gate voltage in either the positive or negative direction, resembling an ambipolar MOS-FET) and unipolar (where the molecule can only be turned on by shifting the gate voltage in the negative direction, resembling an n-type MOS-FET). This study demonstrates that, in addition to molecular structure engineering, molecular electronic functionalities such as tunnelling efficiency and switching behaviour can also be tailored by regulating self-assembly through control of binding preference. These findings suggest a new approach for fabricating advanced quantum technology devices.

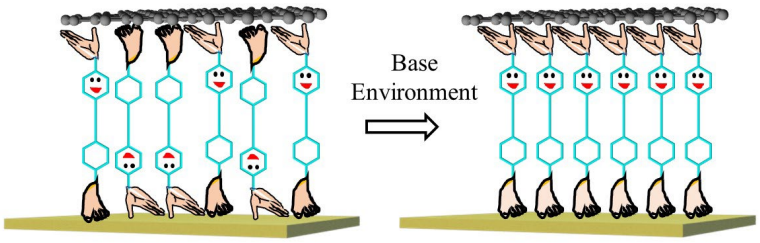

[a.] *College of Environmental Science and Engineering, Dalian Maritime University, Dalian, China*
[b.] *Department of Physics, Cavendish Laboratory, University of Cambridge, Cambridge, CB3 0HE, UK*
[c.] *Zhejiang Mashang Technology Research Institute, Cangnan, Wenzhou, Zhejiang, China*
[d.] *Physics Department, Lancaster University, Lancaster, LA1 4YB, UK.*
[e.] *Department of Physics, College of Education for Pure Science, Tikrit University, Tikrit, Iraq.*
† These authors contributed equally to this work
Electronic Supplementary Information (ESI) available: [details of any supplementary information available should be included here]. See DOI: 10.1039/x0xx00000x

Please do not adjust margins

Introduction

Molecular electronics aim to utilize molecules as functional building blocks for designing electronic devices like logic gates[1, 2], memory devices[3, 4, 5], sensors[6, 7], and thermoelectric harvesters[8-11]. To effectively incorporate functional molecules into circuits[12-14], it is crucial to understand the relationship between the electronic properties of molecules and their structure, particularly the anchor groups that establish contact with external electrodes. Molecular backbones with asymmetric anchors at both terminals are of great interest due to their unique properties, like rectification and tunable thermoelectric behaviors[15-21]. This is because the presence of an asymmetric anchor/electrode interface not only leads to an asymmetric coupling strength between the molecule and the electrodes[17, 18] but also influences the energy difference between the electrode Fermi level and the frontier molecular orbital[19-21]. The electron transport properties of asymmetrically anchored molecules have been extensively investigated at both the single-molecule[17, 18, 22-24] and SAMs scale. In SAMs, due to the strong affinity of both terminals of asymmetrically anchored molecular wires to the substrate, the wires can attach to the substrate in either orientation. However, there have been limited studies focusing on how this mix in orientation affects the SAMs transport behaviour. Nevertheless, understanding its effect is crucial since the substrate-molecule interface significantly determines the mode of molecular electron tunnelling.

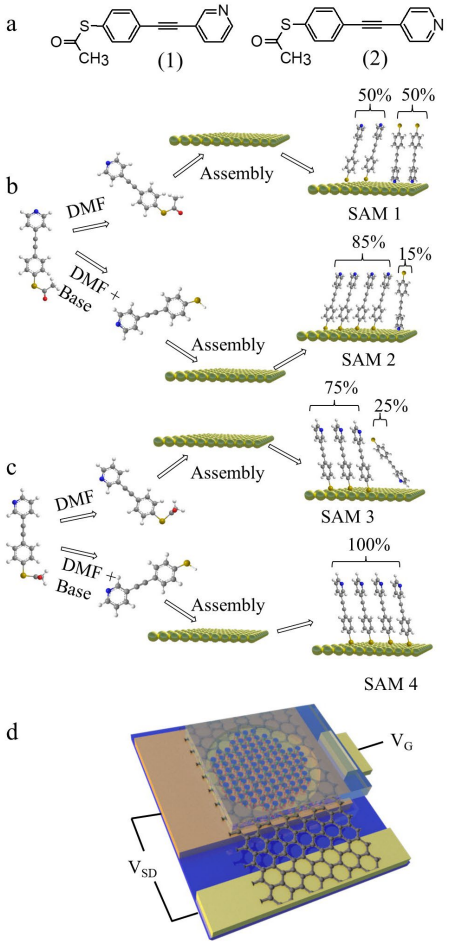

Figure 1. Molecules (a), assembly of SAMs (b, c, SAM **1-4**), and device structure in this work (d).

In this study, we investigated two types of Oligo (arylene ethynylene) (OAEs) molecular wires, as shown in Fig. 1(a), that possess a thiol acetate group at one end and a pyridine group at the other end. These molecules were assembled onto our previously reported micro-well chip with a gold bottom electrode and graphene as the top electrode (the fabrication procedure is detailed in the supplementary information, Fig.s S1-S3) [25]. Both pyridine and thiol acetate are known to exhibit strong binding affinity towards the bottom gold electrode[26-30]. Our quantum calculations revealed that the system's minimum energy, Δ(z), for thiol-Au was 0.69 eV, while for pyridine-Au was 0.42 eV, at the optimum distance (refer to the supplementary information for more details). Furthermore, pyridine and graphene exhibited a Δ(z) value of 0.14 eV, due to the nitrogen group of pyridine interacts with graphene through non-covalent van der Waals forces, as previously reported by other research groups[31-33]. By hydrolyzing the

This journal is © The Royal Society of Chemistry 20xx

Please do not adjust margins

Please do not adjust margins

acetyl protection group on the thiol, we achieved the tuning of the molecular anchor binding preference towards the gold substrate from a mixture of half thiol anchor and half pyridine anchor to almost 100% thiol-anchored (as shown in Fig. 1(b, c)). Additionally, we utilized an ionic liquid (DEME-TFSI) as the gate (as depicted in Fig. 1(d)) to establish a correlation between this binding preference and both the electron tunneling efficiency and the alignment of the electrode Fermi level[25]. The results demonstrate that, in addition to molecular structure engineering, regulating the molecular orientational preference by altering the assembly conditions while writing molecules into electric circuits can be another effective method for imparting novel functionalities.

Results and Discussion

Molecular wires containing a thiol acetate anchor group have the ability to directly form self-assembled monolayers (SAMs) on gold substrates through the formation of an Au/S bond. During this process, the acetyl group is spontaneously released [29, 30, 34]. However, it has been observed that the quality of these SAMs is relatively low[30, 34-36]. Further investigations have demonstrated that by introducing a base into the molecular solution, the acetyl group can be cleaved off, resulting in the transfer of the thiol acetate anchor to a thiol anchor. This modification facilitates the attachment of sulfur (S) to gold (Au), thereby enhancing the formation of high-quality SAMs [35, 36].

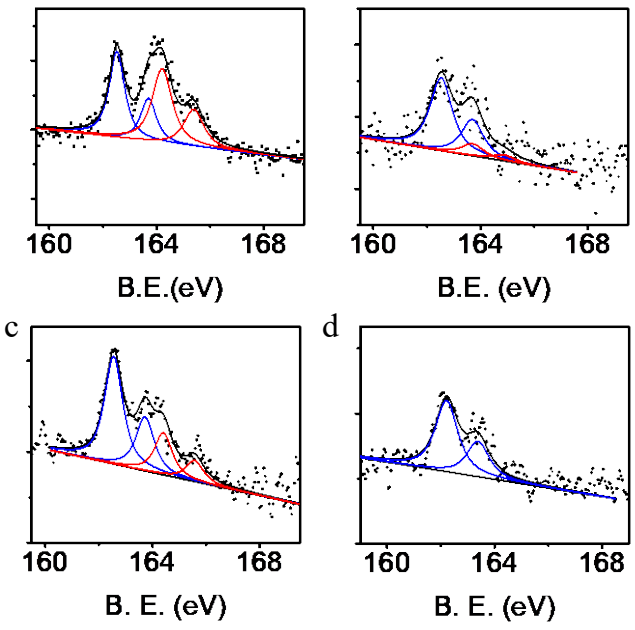

Figure 2. XPS result of S2p signal for SAMs **1-4** (a - d).

In this study, we grew asymmetrically anchored self-assembled monolayers (SAMs) on a gold electrode, and characterized their growing status using X-ray photoelectron spectroscopy (XPS). Fig. 2 presents the results of the sulfur 2p orbital (S2p) signal obtained for the four types of SAMs shown in Fig. 1b. SAMs **1** and **2** were grown using molecules with thiol acetate anchors and nitrogen in pyridine anchors in the para position (Fig. 1a (1)). SAM **1** was produced by directly dipping the device into the molecular solution, while SAM **2** was grown by dipping the device into a molecular solution with base deprotection (detailed procedure explained in SI, and Fig. S4 shows that deprotection did not introduce additional contaminants to the SAMs). SAMs **3** and **4** were similar but had the pyridine nitrogen and thiol acetate in the meta position (Fig. 1a (2)).

A typical S2p XPS signal consists of a doublet peak with a peak separation of 1.16 eV and an intensity ratio of 2:1, which arises from spin-orbit splitting ($S2p_{\frac{1}{2}}$ and $S2p_{\frac{3}{2}}$) [37]. The XPS analysis of SAM **1** (Fig. 1b) revealed two S2p signals. The first S2p signal with the $S2p_{\frac{3}{2}}$ peak located at approximately 162 eV (blue curve), which is a characteristic feature of thiolate groups bonded with the Au substrate[38, 39]. This corresponds to the molecules standing on the Au substrate with their thiol anchor, and we refer to them as "foot-standing" molecules. The second S2p signal exhibited the $S2p_{\frac{3}{2}}$ peak located at approximately 164 eV (red curve), which is typical of thiolate groups not bonded with gold (free thiolates)[38, 39]. This corresponds to the molecules standing on the Au substrate with their pyridine anchor, resulting in free thiolates, and we refer to them as "hand-standing" molecules. The intensities of the Au-bonded thiols and free thiols were nearly equal. This indicates that for SAM **1**, thiol acetate and pyridine have similar affinities for binding sites on gold, resulting in an even distribution of "foot-standing" and "hand-standing" molecules. A similar analysis for SAM **2** showed that 85% of the molecules were "foot-standing" while 15% were "hand-standing". This suggests that cleaving off the acetyl group increased the thiol group's competitiveness for gold binding sites, favouring the "foot-standing" conformation over the "hand-standing" conformation.

SAM **3** was similar to SAM 1, but the pyridine nitrogen was in the meta position. Although these anchors were similar, changing the nitrogen position resulted in a decrease in the ratio of "hand-standing" molecules from 50% to 25%. This implies that meta-pyridine is less competitive than para-pyridine or thiol acetate for binding to gold sites. When thiol acetate was replaced with thiol by adding a base (SAM 4), only a single S2p signal at approximately 162 eV was observed. This indicates that all the molecules adopted a "foot-standing" configuration because the thiol group demonstrated superior affinity compared to the meta-pyridine anchoring group for gold.

This journal is © The Royal Society of Chemistry 20xx

Please do not adjust margins

Please do not adjust margins

Finally, we investigated the S2p signal of a gold piece treated with all device fabrication procedures and immersed in DMF solvent without SAM molecules, and no signal was detected (Fig. S5). This confirms that no sulphur-containing contaminants were introduced during the device fabrication and SAM growth process, validating that the observed sulphur signal originated solely from the molecules. The S:C ratio obtained from XPS measurements also aligns with the expected values (Table S3). Together with the conclusion that all sulfur signals originate from the molecules, we can confirm that all carbon signals are also from the molecules. This indicates the absence of carbon contamination within our SAM system.

The quantum tunnelling behaviour of SAM **1-4** in micro-chip device were investigated both via theoretical and experimental approach. For theoretical calculation, 4 types of junctions were modelled using a combination of density functional theory (DFT) and quantum transport theory (Structure and orbital information of molecules were shown in Fig. S10-S12). To simulate the electron transport [40-42] through SAMs, we modelled the three-terminal junction shown in the top panels of Figs. S19-S21 (with detailed explanation in SI, section 2.7). The optimal binding distances between the electrodes and the different anchor groups were obtained by calculating their binding energies as a function of distance [43, 44], as shown in Figs. S13-S16. The data are summarized in Table S3. The resulting transmission coefficients were shown in Figs. S19-S21, and Table 1.

For experimental investigation, a piece of SLG was transferred onto SAMs as top electrode to form Au/SAM/SLG junction. Voltage sweep by source meter (V_{SD}) was applied between Au and graphene to drive the tunnelling current, and an oscillating voltage with small range ($\pm$5 mV) was floated on V_{SD} to obtain the corresponding differential conductance (G).

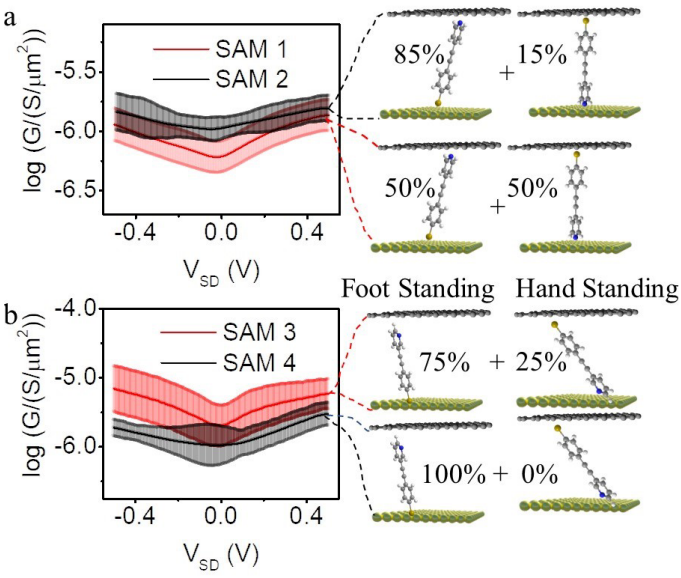

Figure 3. Electric conductance of Au/SAM/SLG junction for SAM **1** – **4** (a, b).

Raman spectra of the transferred graphene on the device (Fig. S7a) showed a 2D/G peak ratio of approximately 2, confirming that the graphene was single-layered. The intensity of the D peak was very small, indicating the absence of significant structural defects on the graphene surface. Fig. S7b shows an AFM topography image of the graphene, revealing the presence of some PMMA residues. It is worth noting that these impurities are extremely difficult to completely remove. In Fig. S7c, we present our micro-well device without functional molecules in-between, and using ionic liquid as the gate. At zero source-drain bias, a conductance dip was observed at 0.5 V (Fig. S7d), suggesting that the impurities functioned as p-type dopants in the graphene. This is consistent with previously published results. The conductance of the Au/SLG junction ranged from 0.1 to 1 mS, which was approximately 100 times higher than the Au/SAM/SLG junctions measured in this study. This difference also served as a means to identify whether the Au/SAM/SLG junction was functioning correctly or if it was a short circuit.

For Au/SAM/SLG junction, at least 2 micro-well device fabricated independently with same recipe was used for electric measurement, and each device contain 16 junctions. The amount of open circuit junction, short circuit junction and survive junction were listed in Table S1. According to the result, SAM **3** shown highest short circuit probability for every device (56% and 31%). This was because meta-pyridine was not a good anchor for gold substrate (as discussed in XPS data analysis), and the SAM anchored with meta-pyridine (hand standing ones) have high possibility of forming defects, which allowed graphene to directly contact with gold and result in short circuit. For SAM **4** the short circuit probability decreased to 0% and 25%, more than 75% of junctions were surviving.

This journal is © The Royal Society of Chemistry 20xx

Please do not adjust margins

Please do not adjust margins

This was because hydrolysis of acetate group let all SAM molecules to anchor with thiol group and formed a uniform "foot standing" SAM instead of a mixed SAM with "foot" and "hand" standing. This significantly increased the SAM quality and enhanced the surviving rate. The surviving rates for both SAM **1** and SAM **2** excessed 69%, with later in average slightly higher than former (75% and 81% respectively). This was expected because it has been reported that treating SAc anchor with weak base can enhance SAM quality, thus decrease the risk of short circuit[36]. Finally, the surviving rate for SAM **1** (ranging from 69% to 87%) was significantly higher than SAM **3** (44% and 69%). This was expected to be the result from binding geometry. Since the lone pair for nitrogen was orthogonal to the π channel of molecular wire [45], "hand standing" molecules in SAM **1** will bind perpendicular to gold substrate. This will facilitate the intermolecular interaction (like π-π interaction) between the molecular wires and let it packing closely with its neighbors [46], thus decreased the possibility of defect formation as argued for SAM**3**. Our previous reported result showing averaged thickness of SAM **1** was higher than SAM **3** further supports this argument [25].

It is important to mention that SAM quality not only determines the survival rate of the devices, but also playing an important role in transport behaviour, particularly in large-scale SAMs like the case demonstrated in this study. The presence of defects and impurities significantly affects key parameters like conductance [47, 48], tunnelling decay coefficient [49], and rectification ratio [50], thereby exerting a significant influence on the overall transport performance of the junction.

Table 1. Theoretical and measured electric conductance ratios for SAM **1-4** at near 0 V_{SD}. ($R=G/G_{Graphene}$, and theory simulations at E_F-E_F^{DFT}=+0.25 eV).

SAM	Foot : Hand	$R_{Exp.\ G}$	$R_{Theo.\ G/Go}$	
			G_{foot}	G_{hand}
1	50:50	(5.3±1.6)E-3	1.7E-2	1.1E-2
2	85:15	(1.0±0.2)E-2		
3	75:25	(2.3±0.4) E-2	2.2E-2	1.4E-2
4	100:0	(1.2±0.4)E-2		

Fig. 3 illustrates the differential conductance for SAMs 1-4, with results compared to theoretical calculations presented in Table 1. It has been demonstrated that the flatness of the gold substrate significantly influences the quantum transport properties of the SAMs [51, 52]. In this study, a thermally-evaporated gold substrate with an average roughness of 1.6±0.3 nm was employed as the bottom substrate (Fig. S3b and S3d). After transferring the graphene as the top electrode, the average roughness decreased to 0.4±0.1 nm (Fig. S3c and S3e). This indicates that the rigid structure of graphene does not conform perfectly to the topography of the bottom gold substrate. This will be leading to contact issues. Several studies have reported that for large-area junctions, the effective electric contact area is typically much smaller (10^2 to 10^5 times) than the geometric contact area [53, 54]. This disparity makes the measured electrical results incomparable with calculated theoretical values. In Table 1, we use conductance ratio, R, instead of absolute conductance G for experiment and theory comparison. The conductance of Au/Graphene junction without SAM was assigned to be 1, and conductance of all junctions was relative to it ($R = \frac{G_{Junction}}{G_{Graphene}}$). The absolute values for SAM conductance were listed in Table S2. For molecule **1** (Fig. 1 (a)), the conductance of SAM obtained from direct growth in DMF (SAM **1**) was about 2 times lower than the one with addition of base (SAM **2**). This outcome was anticipated, as it aligns with both previous reports[15, 55] and the theoretical calculation from this study (Table 1). It is proved that the interfacial electron tunneling efficiency for Au/S bonds is higher than that for Au/Pyridine bonds. This discrepancy arises from the fact that physiosorbed molecules exhibit lower conductivity compared to chemisorbed ones. Compare with SAM **1**, SAM **2** has more molecule forming Au/S bond and less molecule forming Au/pyridine bond, this means its average interfacial tunnelling efficiency was higher and resulted in higher conductance. Interestingly, molecule **2** (Fig. 1 (a)) behaves oppositely to molecule **1**, where SAM without protection group cleavage (SAM **3**, 75% "foot standing") was about 2 times higher than the one with protection group cleavage by base (SAM **4**, 100% "foot standing"). This disagreed with the theoretical approach, which predict the conductance of molecule with "foot standing" was higher than the one with "hand standing" (Table 1). This could due to SAM quality issue. Different from single molecular junction, the electron tunnelling behavior for SAMs was determined not only by molecular layer, but also by defects and pinholes. Especially for low quality SAMs at large junction area, defects might play an important role in electron transport process[50]. Since SAM **3** was low in quality as pre-argued, the defect might influence the electron transfer process and thus increased the measured conductance. For SAM **4**, since all molecules were bind on gold with thiol and formed uniform SAMs, the effect from pinhole or defect was negligible, and the measured conductance was lower than SAM **3**. While compare SAM **2** and SAM **4**, in both SAMs, almost all molecules were anchored on gold with thiol terminal, and the main difference between them was the graphene/molecule interface, SAM **2** molecule contact with graphene by pyridine in para position whereas SAM **3** contact with graphene by pyridine in meta position. Although different in top contact situation, the conductance of SAM **2** and SAM **4** was almost identical (1.0±0.2 and 1.2±0.4 in ratio), and also similar to our reported SAM with similar

Please do not adjust margins

Please do not adjust margins

junction structure, but molecule terminated with thiol acetate at one end and benzene at the other end (1.2±0.2 in ratio, 100% molecules anchored with thiol) [25]. This means in this work, Au/molecule interface determines the electron tunnelling efficiency, and graphene/molecule interface have little impact on total conductance. One reason could be because molecule/Au coupling (chemical adsorption) in this work was much stronger than molecule/graphene coupling (physical contact), so it dominates the electron transport process. The conductance-area analysis was performed on our micro-chip device after SAM growth. The micro-wells of our device were purposely designed to have varied well areas (Figure S10a). In a uniform SAM, the well area should be proportional to the number of molecules in the junction, thereby leading to a proportional relationship with the measured dI/dV due to the parallel alignment of molecular wires in the junction. Figures S10(b-d) demonstrate the near-linear relationship between the well area and the measured dI/dV for SAMs 1-4, confirming the relatively good quality of the SAMs. This linear trend indicates that pinholes and contaminant effects are unlikely, as they occurred randomly instead.

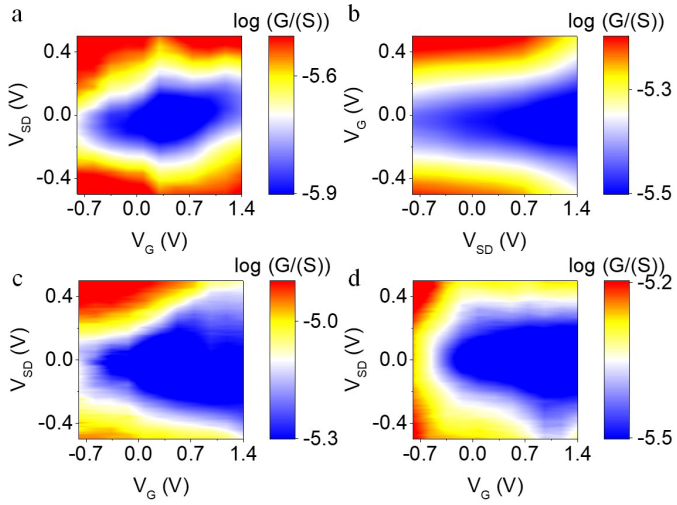

Figure 4. Shift of SAM conductance, G, vs. source drain voltage (V_{SD}) and gate voltage (V_G) for SAM **1-4** (a-d).

An essential challenge for investigating electron tunnelling behavior of SAMs is to shift the energetic position of electrode Fermi level toward molecular frontier orbital. Our group successfully demonstrated a way of using single layered graphene as top electrode and ionic liquid as gate to achieve this goall[25]. Since graphene is ultra-thin, gate voltage can partially penetrate through it and tunned the molecular orbital alignment of SAM molecules beneath it [56-59]. Fig. 4 shown the conductance shift of SAM by sweeping the source drain voltage (V_{SD}) and gate voltage (V_G). The most interesting observation was the gating behavior different between SAM **1** and **2**. For SAM1 (molecule **1** growth without protection group cleavage), the G vs. V_{SD} vs. V_G shown ambipolar behavior (Fig. 4(a)), with lowest conductance at $V_G \sim 0.2$ V, and increased as gate voltage swept either toward positive or negative, which function as an ambipolar molecular metal-insulator-semiconductor field effect transistor (ambipolar MMIS-FET). This indicated that the Fermi level of electrode is siting close to the dip of HOMO-LUMO gap, thus either Fermi level swept toward HOMO or LUMO resonance, the density of state (DOS) increased and thus molecular conductance increased as well (Fig. S8). However, for molecule 1 with protection group cleavage (SAM **2**), its G vs. V_{SD} vs. V_G performance changed from ambipolar to unipolar (Fig. 4(b)) in same gate voltage sweeping range. The conductance increased as gate voltage swept from positive to negative, which function as a n-type MMIS-FET. This indicates for SAM **2**, Fermi level located close to the HOMO resonance, so for positive gate voltage Fermi level shifted toward the HOMO-LUMO mid gap with lower DOS and for negative voltage, Fermi level shifted toward HOMO resonance with higher DOS (Fig. S9). It has been reported that the relative position between Fermi level and molecular orbital was highly influenced by the anchor group of the molecule [15, 60, 61]. For thiol anchored molecules, since the lone pair of sulphur are coplanar with the π channel of the wire, the Au/S transport is usually π dominated [20, 45]. By contrast, for pyridine anchored molecules, the lone pair of nitrogen is orthogonal to the π channel of the wire and the π^* orbital is more significant [62]. This means in normal case, electron transport for molecules anchor on gold with thiol (foot standing molecules) was HOMO dominated and the ones anchor with pyridine (hand standing molecules) was LUMO dominated. For SAM **2**, most molecules were "foot standing", and the effect from the "hand standing" molecules were almost negligible, so it behaved as HOMO dominated junction. For SAM **1**, "hand standing" molecules and "foot standing" molecules were in a ratio of 1:1, "hand standing" ones were no longer negligible, they introduce additional resonance close to the Fermi level in high energy direction and result in ambipolar behaviour. For SAM **3** and **4**, since most molecules were in "foot standing" form, they exhibit HOMO dominated behaviour (Fig. 4 (c) and (d)). It is worth mentioning that there is a possibility of ions from the ionic liquid penetrating through the graphene layer and doping the self-assembled monolayer. To investigate this, we measured the IV characteristics of the device before adding the ionic liquid, after adding the ionic liquid, and after completing the gate voltage (GV) measurement. The resulting IV curves from these three stages exhibited similar behavior (Figure S6), confirming that the presence of the ionic doping did not significantly affect the outcomes of this study. Furthermore, the voltage between the source and gate also demonstrated minimal current leakage

This journal is © The Royal Society of Chemistry 20xx

Please do not adjust margins

Please do not adjust margins

within the range employed for the gate behavior measurement (Figure S5).

Conclusions

In summary, we have successfully achieved control over the directional preference of asymmetrically anchored molecules self-assembled on a gold substrate by regulating their binding competitiveness. This control has allowed us to manipulate the electron tunneling efficiency and Fermi-level alignment of the investigated junctions. Our findings not only provide novel insights into precise self-assembly control but also offer valuable guidance for bottom-up fabrication in the advancement of next-generation molecular electronic devices. Additionally, this work highlights the significance of molecule-electrode coupling strength in optimizing junction performance, which aligning with previous reports [32, 63]. Moving forward, we will place particular focus on studying this aspect in our future research.

Author Contributions

A.K.I and X.W. conceived the research. A.K.I. carried out the calculations. X.W., X.L., and S.N. performed device design, fabrication and measurements. All co-authors assisted in writing the manuscript. X.W. and A.K.I. supervised the research and provided essential contributions to interpreting the results and drafting the manuscript.

Conflicts of interest

We declare that we have no conflict of interest.

Acknowledgements

This work was supported by the UK EPSRC (grants EP/P027156/1, EP/P027172/1 and EP/P027520/1) and National Youth Talent Program of China. A.K.I. acknowledges the Leverhulme Trust for Early Career Fellowship ECF-2020-638. A.K.I acknowledge financial support from the UK EPSRC (grants EP/M014452/1 and EP/N03337X/1). This work was additionally funded by the European Commission FET Open projects 767187-QuIET and 766853-EFINED, and the EU project Bac-to-Fuel. A.K.I is grateful for financial assistance from Tikrit and Anbar Universities (Iraq), and the Iraqi Ministry of Higher Education (SL-20). X.W. acknowledge financial support from China National Youth Talent Program.

References

1. N. Zhang, W. Y. Lo, A. Jose, Z. X. Cai, L. W. Li and L. P. Yu, *Adv Mater*, 2017, **29**, 1701248.
2. O. F. Namarvar, O. Giraud, B. Georgeot and C. Joachim, *Quantum Sci Technol*, 2019, **4**, 035009.
3. J. Lee, H. Chang, S. Kim, G. S. Bang and H. Lee, *Angewandte Chemie-International Edition*, 2009, **48**, 8501-8504.
4. J. Y. Hong, S. H. Chang, K. H. O. Yang, P. C. Yeh, H. W. Shiu, C. H. Chen, W. C. Chiang and M. T. Lin, *J Appl Phys*, 2019, **125**, 142905.
5. Y. M. Han, C. Nickle, Z. Y. Zhang, H. P. A. G. Astier, T. J. Duffin, D. C. Qi, Z. Wang, E. del Barco, D. Thompson and C. A. Nijhuis, *Nat Mater*, 2020, **19**, 843-848.
6. G. Seo, G. Lee, M. J. Kim, S. H. Baek, M. Choi, K. B. Ku, C. S. Lee, S. Jun, D. Park, H. G. Kim, S. J. Kim, J. O. Lee, B. T. Kim, E. C. Park and S. I. Kim, *Acs Nano*, 2020, **14**, 5135-5142.
7. Y. Fujimoto, *Mod Phys Lett B*, 2021, **35**, 2130001.
8. X. T. Wang, A. Ismael, A. Almutlg, M. Alshammari, A. Al-Jobory, A. Alshehab, T. L. R. Bennett, L. A. Wilkinson, L. F. Cohen, N. J. Long, B. J. Robinson and C. Lambert, *Chem Sci*, 2021, **12**, 5230-5235.
9. X. T. Wang, S. Sangtarash, A. Lamantia, H. Dekkiche, L. Forcieri, O. V. Kolosov, S. P. Jarvis, M. R. Bryce, C. J. Lambert, H. Sadeghi and B. J. Robinson, *J Phys-Energy*, 2022, **4**, 024002.
10. S. Park and H. J. Yoon, *Nano Lett*, 2018, **18**, 7715-7718.
11. Y. Kim, W. Jeong, K. Kim, W. Lee and P. Reddy, *Nat Nanotechnol*, 2014, **9**, 881-885.
12. B. Limburg, J. O. Thomas, G. Holloway, H. Sadeghi, S. Sangtarash, I. C. Y. Hou, J. Cremers, A. Narita, K. Mullen, C. J. Lambert, G. A. D. Briggs, J. A. Mol and H. L. Anderson, *Adv Funct Mater*, 2018, **28**, 1803629.
13. E. Lortscher, C. J. Cho, M. Mayor, M. Tschudy, C. Rettner and H. Riel, *Chemphyschem*, 2011, **12**, 1677-1682.
14. F. Xie, Z. Q. Fan, K. Q. Chen, X. J. Zhang and M. Q. Long, *Org Electron*, 2017, **50**, 198-203.
15. A. Ismael, X. T. Wang, T. L. R. Bennett, L. A. Wilkinson, B. J. Robinson, N. J. Long, L. F. Cohen and C. J. Lambert, *Chem Sci*, 2020, **11**, 6836-6841.
16. S. Parashar, P. Srivastava and M. Pattanaik, *Solid State Commun*, 2014, **191**, 54-58.
17. K. Wang, J. F. Zhou, J. M. Hamill and B. Q. Xu, *J Chem Phys*, 2014, **141**, 054712.
18. Y. Komoto, S. Fujii and M. Kiguchi, *Adv Nat Sci-Nanosci*, 2017, **8**, 025007.
19. T. L. R. Bennett, M. Alshammari, S. Au-Yong, A. Almutlg, X. T. Wang, L. A. Wilkinson, T. Albrecht, S. P. Jarvis, L. F. Cohen, A. Ismael, C. J. Lambert, B. J. Robinson and N. J. Long, *Chem Sci*, 2022, **13**, 5176-5185.
20. X. T. Wang, T. L. R. Bennett, A. Ismael, L. A. Wilkinson, J. Hamill, A. J. P. White, I. M. Grace, O. V. Kolosov, T. Albrecht, B. J. Robinson, N. J. Long, L. F. Cohen and C. J. Lambert, *J Am Chem Soc*, 2020, **142**, 8555-8560.
21. L. A. Wilkinson, T. L. R. Bennett, I. M. Grace, J. Hamill, X. T. Wang, S. Au-Yong, A. Ismael, S. P. Jarvis, S. J. Hou, T. Albrecht, L. F. Cohen, C. Lambert, B. J. Robinson and N. J. Long, *Chem Sci*, 2022, **13**, 8380-8387.
22. C. J. Xia, H. C. Liu and Y. T. Zhang, *Solid State Phenomen*, 2012, **181-182**, 344-347.
23. C. H. He, Q. Zhang, Y. Q. Fan, C. Z. Zhao, C. Zhao, J. Y. Ye, Y. J. Dappe, R. J. Nichols and L. Yang, *Chemphyschem*, 2019, **20**, 1830-1836.
24. S. Martin, D. Z. Manrique, V. M. Garcia-Suarez, W. Haiss, S. J. Higgins, C. J. Lambert and R. J. Nichols, *Nanotechnology*, 2009, **20**, 125203.

Please do not adjust margins

Please do not adjust margins

25. X. T. Wang, A. Ismael, S. L. Ning, H. Althobaiti, A. Al-Jobory, J. Girovsky, H. P. A. G. Astier, L. J. O'Driscoll, M. R. Bryce, C. J. Lambert and C. J. B. Ford, *Nanoscale Horiz*, 2022, **7**, 1201-1209.
26. Y. Ie, T. Hirose, H. Nakamura, M. Kiguchi, N. Takagi, M. Kawai and Y. Aso, *J Am Chem Soc*, 2011, **133**, 3014-3022.
27. S. Ballmann, W. Hieringer, R. Hartle, P. B. Coto, M. R. Bryce, A. Gorling, M. Thoss and H. B. Weber, *Phys Status Solidi B*, 2013, **250**, 2452-2457.
28. H. Ozawa, M. Baghernejad, O. A. Al-Owaedi, V. Kaliginedi, T. Nagashima, J. Ferrer, T. Wandlowski, V. M. Garcia-Suarez, P. Broekmann, C. J. Lambert and M. Haga, *Chem-Eur J*, 2016, **22**, 12732-12740.
29. L. J. Cui, R. J. Miao, K. Wang, D. Thompson, L. A. Zotti, J. C. Cuevas, E. Meyhofer and P. Reddy, *Nat Nanotechnol*, 2018, **13**, 122-127.
30. T. Park, H. Kang, S. Seong, S. Han, Y. J. Son, E. Ito, T. Hayashi, M. Hara and J. Noh, *J Phys Chem C*, 2019, **123**, 9096-9104.
31. S. Park, H. R. Kim, J. Kim, B. H. Hong and H. J. Yoon, *Adv Mater*, 2021, **33**, 2103177.
32. P. Song, C. S. S. Sangeeth, D. Thompson, W. Du, K. P. Loh and C. A. Nijhuis, *Adv Mater*, 2016, **28**, 631-639.
33. B. Long, M. Manning, M. Burke, B. N. Szafranek, G. Visimberga, D. Thompson, J. C. Greer, I. M. Povey, J. MacHale, G. Lejosne, D. Neumaier and A. J. Quinn, *Adv Funct Mater*, 2012, **22**, 717-725.
34. Z. M. Wei, T. Hansen, M. Santella, X. T. Wang, C. R. Parker, X. B. Jiang, T. Li, M. Glyvradal, K. Jennum, E. Glibstrup, N. Bovet, X. W. Wang, W. P. Hu, G. C. Solomon, M. B. Nielsen, X. H. Qiu, T. Bjornholm, K. Norgaard and B. W. Laursen, *Adv Funct Mater*, 2015, **25**, 1700-1708.
35. Z. M. Wei, T. Li, K. Jennum, M. Santella, N. Bovet, W. P. Hu, M. B. Nielsen, T. Bjornholm, G. C. Solomon, B. W. Laursen and K. Norgaard, *Langmuir*, 2012, **28**, 4016-4023.
36. H. Valkenier, E. H. Huisman, P. A. van Hal, D. M. de Leeuw, R. C. Chiechi and J. C. Hummelen, *J Am Chem Soc*, 2011, **133**, 4930-4939.
37. T. B. Creczynski-Pasa, M. A. D. Millone, M. L. Munford, V. R. de Lima, T. O. Vieira, G. A. Benitez, A. A. Pasa, R. C. Salvarezza and M. E. Vela, *Phys Chem Chem Phys*, 2009, **11**, 1077-1084.
38. C. Vericat, M. E. Vela, G. Benitez, P. Carro and R. C. Salvarezza, *Chem Soc Rev*, 2010, **39**, 1805-1834.
39. T. Ishida, N. Nishida, S. Tsuneda, M. Hara, H. Sasabe and W. Knoll, *Jpn J Appl Phys 2*, 1996, **35**, L1710-L1713.
40. A. K. Ismael and C. J. Lambert, *Nanoscale Horiz*, 2020, **5**, 1073-1080.
41. A. Alshehab and A. K. Ismael, *Rsc Adv*, 2023, **13**, 5869-5873.
42. M. Alshammari, A. A. Al-Jobory, T. Alotaibi, C. J. Lambert and A. Ismael, *Nanoscale Adv*, 2022, **4**, 4635-4638.
43. J. M. Hamill, A. Ismael, A. Al-Jobory, T. L. R. Bennett, M. Alshahrani, X. T. Wang, M. Akers-Douglas, L. A. Wilkinson, B. J. Robinson, N. J. Long, C. Lambert and T. Albrecht, *J Phys Chem C*, 2023, **127**, 7484-7491.
44. M. T. Gonzalez, A. K. Ismael, M. Garcia-Iglesias, E. Leary, G. Rubio-Bollinger, I. Grace, D. Gonzalez-Rodriguez, T. Torres, C. J. Lambert and N. Agrait, *J Phys Chem C*, 2021, **125**, 15035-15043.
45. T. A. Su, M. Neupane, M. L. Steigerwald, L. Venkataraman and C. Nuckolls, *Nat Rev Mater*, 2016, **1**, 16002.
46. R. F. Dou, X. C. Ma, L. Xi, H. L. Yip, K. Y. Wong, W. M. Lau, J. F. Jia, Q. K. Xue, W. S. Yang, H. Ma and A. K. Y. Jen, *Langmuir*, 2006, **22**, 3049-3056.
47. A. Vilan, D. Aswal and D. Cahen, *Chem Rev*, 2017, **117**, 4248-4286.
48. J. Ru, B. Szeto, A. Bonifas and R. L. McCreery, *Acs Appl Mater Inter*, 2010, **2**, 3693-3701.
49. L. Yuan, L. Jiang, B. Zhang and C. A. Nijhuis, *Angewandte Chemie-International Edition*, 2014, **53**, 3377-3381.
50. X. P. Chen, H. T. Hu, J. Trasobares and C. A. Nijhuis, *Acs Appl Mater Inter*, 2019, **11**, 21018-21029.
51. S. K. Karuppannan, H. T. Hu, C. Troadec, A. Vilan and C. A. Nijhuis, *Adv Funct Mater*, 2019, **29**, 1904452.
52. W. X. Peng, Z. Cao, N. Y. Chen, Y. Xie and Y. Li, *J Mater Chem A*, 2022, **10**, 23304-23313.
53. S. K. Karuppannan, E. H. L. Neoh, A. Vilan and C. A. Nijhuis, *J Am Chem Soc*, 2020, **142**, 3513-3524.
54. F. C. Simeone, H. J. Yoon, M. M. Thuo, J. R. Barber, B. Smith and G. M. Whitesides, *J Am Chem Soc*, 2013, **135**, 18131-18144.
55. M. Saitner, F. Eberle, J. Baccus, M. D'Olieslaeger, P. Wagner, D. M. Kolb and H. G. Boyen, *J Phys Chem C*, 2012, **116**, 21810-21815.
56. T. Georgiou, R. Jalil, B. D. Belle, L. Britnell, R. V. Gorbachev, S. V. Morozov, Y. J. Kim, A. Gholinia, S. J. Haigh, O. Makarovsky, L. Eaves, L. A. Ponomarenko, A. K. Geim, K. S. Novoselov and A. Mishchenko, *Nat Nanotechnol*, 2013, **8**, 100-103.
57. T. Tian, P. Rice, E. J. G. Santos and C. J. Shih, *Nano Lett*, 2016, **16**, 5044-5052.
58. M. Famili, C. C. Jia, X. S. Liu, P. Q. Wang, I. M. Grace, J. Guo, Y. Liu, Z. Y. Feng, Y. L. Wang, Z. P. Zhao, S. Decurtins, R. Haner, Y. Huang, S. X. Liu, C. J. Lambert and X. F. Duan, *Chem-Us*, 2019, **5**, 474-484.
59. C. C. Jia, M. Famili, M. Carlotti, Y. Liu, P. Q. Wang, I. M. Grace, Z. Y. Feng, Y. L. Wang, Z. P. Zhao, M. N. Ding, X. Xu, C. Wang, S. J. Lee, Y. Huang, R. C. Chiechi, C. J. Lambert and X. F. Duan, *Sci Adv*, 2018, **4**, 8237.
60. D. D. Zhai, J. P. Wang, L. N. Hao, C. M. Ma, P. Ma, Y. Pan and J. C. Jiang, *Rsc Adv*, 2019, **9**, 37747-37758.
61. Y. Q. Liu, M. Santella, Z. Q. Fan, X. T. Wang, X. W. Jiang, M. B. Nielsen, K. Norgaard, B. W. Laursen, J. B. Li and Z. M. Wei, *Chinese Chem Lett*, 2018, **29**, 271-275.
62. M. Mayor, H. B. Weber, J. Reichert, M. Elbing, C. von Hanisch, D. Beckmann and M. Fischer, *Angewandte Chemie-International Edition*, 2003, **42**, 5834-5838.
63. L. Yuan, N. Nerngchamnong, L. Cao, H. Hamoudi, E. del Barco, M. Roemer, R. K. Sriramula, D. Thompson and C. A. Nijhuis, *Nat Commun*, 2015, **6**, 6324.

 This journal is © The Royal Society of Chemistry 20xx

Please do not adjust margins